Applied Catalysis B: Environmental 192 (2016) 260–267

Contents lists available at ScienceDirect

Applied Catalysis B: Environmental

journal homepage: www.elsevier.com/locate/apcatb

Sulfurized carbon xerogels as Pt support with enhanced activity for fuel cell applications

Cinthia Alegre[a,b], David Sebastián[a,b], María Elena Gálvez[a,c], Rafael Moliner[a], María Jesús Lázaro[a,*]

[a] Instituto de Carboquímica (ICB-CSIC), C/. Miguel Luesma Castán 4, 50018 Zaragoza, Spain
[b] Istituto di Tecnologie Avanzate per l'Energia "Nicola Giordano" (CNR-ITAE), Salita Santa Lucia sopra Contesse, 5, 98126 Messina Italy
[c] UPMC, Univ Paris 06, Sorbonne Universités, Institut Jean Le Rond d'Alembert, 2 Place de la Gare de Ceinture, 78210 Saint Cyr l'Ecole, France

ARTICLE INFO

Article history:
Received 28 November 2015
Received in revised form 23 March 2016
Accepted 30 March 2016
Available online 31 March 2016

Keywords:
Sulfur
Carbon xerogel
Fuel cell
Oxygen reduction reaction
Methanol oxidation reaction

ABSTRACT

Carbon xerogels represent nowadays an outstanding alternative to carbon blacks for the preparation of efficient fuel cell electrocatalysts, due to their easily tunable and well developed mesoporous structure. To further improve both activity and durability of Pt/C catalysts, the introduction of heteroatoms (such as O, N, S, P, B, etc.) in the structure of carbon materials has been proposed. In the present work, highly mesoporous carbon xerogels (CXGs) have been subjected to a sulfurization process with elemental sulfur. The insertion of S into the carbon matrix does not compromise their mesoporous structure. Pt catalysts supported on sulfurized carbon xerogels show enhanced catalytic activity towards both the methanol electro-oxidation and the oxygen electro-reduction reactions, exceeding not only the performance of the catalyst supported on the bare xerogel, but also of the catalyst supported on a commercial carbon black. The sulfurization treatment is also effective in improving the resistance of Pt/CXG catalysts towards corrosion phenomena occurring at the fuel cell cathode.

1. Introduction

Direct methanol fuel cells (DMFCs) have attracted a great deal of attention due to their advantageous characteristics, but the need of precious metal catalysts have delayed their full implementation in the market. Pt-based catalysts present the highest activity towards the oxygen reduction reaction (ORR) and the methanol oxidation reaction (MOR), but due to the prohibitive cost and scarce resources of Pt, an improvement in both activity and stability is still needed [1–4]. An approach to enhance the latter is based on the design of non-conventional catalyst supports, such as transition metal oxides, nitrides and/or carbides [5–7] or advanced carbon supports functionalized or doped with heteroatoms such as oxygen, nitrogen, boron, sulfur, phosphorus, selenium, etc [8–10]. The presence of such heteroatoms modifies the interaction between the metal catalyst and the support, resulting in a more appropriate surface electronic density, better metal dispersion, stability and morphology of metallic crystallites [11,12].

Currently, carbon blacks are well established materials widely used as electrocatalyst support due to their excellent combination of textural and structural properties, which favors the adequate dispersion of the noble metal particles and the electronic transport [9,13]. Due to its low cost and high availability, oil-furnace carbon black (e.g. Vulcan XC-72) has been widely used as the benchmark support for platinum catalyst in low-temperature fuel cells [14]. Carbon blacks are generally characterized by high specific surface area, mostly micropores lower than 1 nm, which are thus more difficult to be fully accessible for platinum deposition and reactant/product diffusion to/from the catalytic active sites. The use of advanced carbon nanomaterials, such as carbon nanotubes/nanofibers, graphene, etc., has provided better performances in comparison to conventional carbon blacks [9,10]. Among these advanced carbon supports, carbon gels have been studied for their unique properties, such as high meso-porosity (>80%), high surface area (400–1200 $m^2\ g^{-1}$) and controlled pore size distributions [15–17]. Within the different types of carbon gels, carbon xerogels (CXGs) are characterized by a simple and cost-effective drying process, rendering them as highly interesting from a practical point of view [17]. Moreover, CXGs have shown improved activity when used as electrocatalyst support, mainly due to the decrease of mass transfer constraints [18–23]. In a recent work, we demonstrated

* Corresponding author.
E-mail address: mlazaro@icb.csic.es (M.J. Lázaro).

http://dx.doi.org/10.1016/j.apcatb.2016.03.070
0926-3373/

Table 1
Elemental analysis of the sulfurized carbon xerogels (wt.%).

	% S	% C	% N	% H
CXG	0	95.3	0.2	0.7
CXG-1S	1.1	94.0	0.2	0.7
CXG-3S	2.8	92.3	0.2	0.7
CXG-5S	4.2	91.8	0.2	0.6
CXG-7S	7.0	88.6	0.3	0.7

that not only the porosity, but also the carbon arrangement, plays a key role on the properties and the electrocatalytic activity of Pt/CXG catalysts [24]. Nevertheless, catalysts supported on CXGs are still prone to corrosion given its amorphous nature, as also stated in a previous work [25]. Improving the resistance to corrosion of CXGs is highly desirable in order to enhance the durability of fuel cells.

Several works have claimed the benefits of doping/treating carbon structures with sulfur in the last decade. Sulfurized porous carbon materials find application in many fields such as electrocatalysts for fuel cells, anode materials in lithium-ion batteries, electrodes in electrochemical capacitors, H_2 storage and CO_2 capture, etc [8,26,27]. In a recent review by Kicinski et al. sulfur-doped porous carbons and some applications are analyzed in detail [26]. Introducing sulfur in the carbonaceous structure has been reported to enhance the anchoring of the metal particles on the support. The chemical bond between the metal particle and sulfur functionalities reduces the effect of dissolution and recrystallization (Ostwald ripening) of the catalyst particles, thus enhancing the resistance to degradation [27].

Up to our knowledge, only few works deal with sulfurized carbon gels [27–29]. Generally, time-consuming procedures and expensive reagents are employed to effectively introduce sulfur within the carbonaceous matrix. For instance, Baker et al. soaked organic gels with a 3-thiophenecarboxaldehyde/phthaloyl dichloride solution for 2 days [27]. After this, the so-called sulfur-doped gel was washed with acetone for three days. Other authors employed the sulfur precursor (for example, thienyl-L-cysteine, 2-thienyl-carboxaldehyde or 2-thiophenecarboxaldehyde) as an addtive to the conventional gelation process, along with resorcinol or other carbon precursors such as glucose [28,29]. In this work, a simple post-treatment procedure based on the sulfurization with elemental sulfur was employed [30–32]. The herein presented methodology allowed the efficient incorporation of S in the carbon matrix without compromising the mesoporous structure of the CXG. As-described sulfurized carbon xerogels (S-CXGs) were investigated as Pt support for fuel cell applications. The correlation of S-CXGs features and the catalytic activity and stability of Pt/S-CXG catalysts was assessed for the methanol oxidation and the oxygen reduction reactions.

2. Experimental

2.1. Carbon xerogel synthesis and sulfurization

Carbon xerogels were synthesized by a sol-gel method as described by Lin and Czakkel [15,33]. Briefly, 0.35 g mL^{-1} resorcinol, 1.16 mg mL^{-1} sodium carbonate and 0.20 g mL^{-1} formaldehyde were stirred for 30 min in deionized water. Subsequently, diluted nitric acid was added until pH 6 was reached. The previous solution was poured into closed vials and the gelification/curing process consisted of 24 h at room temperature followed by 24 h at 50 °C and 72 h at 85 °C. The resulting material was subjected to sub-critical drying in air at 110 °C for 5 h. So-obtained organic xerogels were pyrolyzed in N_2 according to the following temperature steps: 2 h at 150 °C; 1 h at 300 °C; 1 h at 600 °C and 2 h at 800 °C [34].

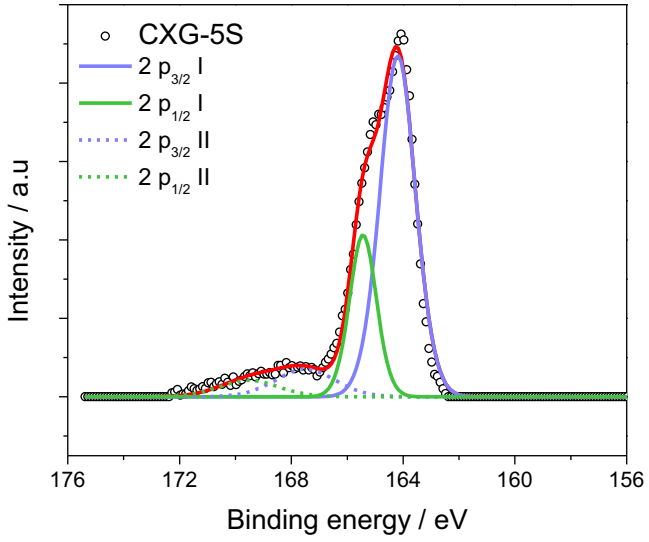

Fig. 1. XPS spectra for the S 2p region for the carbon xerogel CXG-5S.

The sulfurization treatment consisted of physically mixing the carbon xerogel (CXG) with elemental sulfur (99.998% trace metals basis, Sigma-Aldrich). The powder was then subjected to a heat treatment for 12 h in Ar at 160 °C. The appropriate amounts of CXG and sulfur were employed to obtain different compositions with increasing S content from 1 wt.% to 7 wt.%.

2.2. Pt catalysts synthesis

Pt catalysts with a 20 wt.% loading were synthesized using both bare (CXG) and sulfurized carbon xerogels (S-CXGs) as support, by means of a one-step method consisting of impregnation and reduction with formic acid. The Pt content in the catalyst was selected on the basis of previous works [19,24,25,35], being low enough to minimize the relative contribution of Pt nanoparticle dispersion on the electrochemical behavior, and aimed to better individuate the influence of the support [36]. Briefly, the carbon material was first dispersed in a 2 M HCOOH (Panreac) solution in water at 80 °C. Subsequently, a 4 mM aqueous solution of the metallic precursor, H_2PtCl_6 (Sigma-Aldrich), was added dropwise. After completing the addition, the mixture was stirred at 80 °C for 1 h. Finally the catalysts were filtered and thoroughly washed with deionized water, and dried overnight at 60 °C.

2.3. Physico-chemical characterization

The textural and morphological features of the carbon xerogels were determined by means of N_2 physisorption at −196 °C (Micromeritics ASAP 2020). Specific surface area and pore volume were calculated from the adsorption-desorption isotherms applying the Brunauer-Emmet-Teller (BET) equation, Barrett-Joyner-Halenda (BJH) and t-plot methods. The electrical conductivity of CXGs was measured by pressing the carbonaceous powder up to 10 MPa as described elsewhere [37]. The electrical conductivity was determined applying electrical current scans up to 20 mA and measuring the voltage drop. The electrical resistance was then calculated by Ohm's law, where the system resistance was subtracted. The conductivity was then obtained from the sample resistance and geometric considerations [38]. The composition of the CXGs was studied by means of elemental analysis, in a Thermo Flash 1112 analyzer for the determination of C, H, N and S, in a range between 0.05% and 99.95%. X-Ray photoelectron spectroscopy (XPS) was used to analyze the composition and oxi-

Table 2
Atomic percentage of the different groups deconvoluted from the S2p band in the XPS of S-CXGs.

Carbon xerogels	% S	B.E/eV	$S2p_{3/2}$ I	B.E/eV	$S2p_{1/2}$ I	B.E/eV	$S2p_{3/2}$ II	B.E/eV	$S2p_{1/2}$ II
CXG-1S	3.0	164.07	62.5	167.50	23.9	165.31	9.1	169.60	4.4
CXG-3S	6.3	163.81	61.8	167.50	24.6	165.08	9.8	169.82	3.7
CXG-5S	8.1	164.19	63.1	167.50	22.6	165.43	9.6	169.99	4.7
CXG-7S	13.7	164.13	65.0	167.50	22.3	165.38	8.6	169.93	4.2

dation state of both carbon xerogels and Pt catalysts. An ESCAPlus Omicron spectrometer was used, equipped with a Mg (1253.6 eV) anode, 150 W (15 mA, 10 kV) power, over an area of sample of 1.75 × 2.75 mm. Signals were obtained at 0.1 eV step, 0.5 s dwell and 20 eV pass energy, analyzing the S 2p and Pt 4f bands. Spectra were deconvoluted using CasaXPS software. A Shirley-type background correction was used for the quantification of the spectra, considering a 70% Gaussian and 30% Lorentzian line shape in the curve fitting of the high resolution peaks, a standard deviation of ±0.25 eV, and sensitivity factors provided by the manufacturer. X-ray diffraction (XRD) analyses were obtained using a Bruker AXS D8 Advance diffractometer, with a θ-θ configuration and using Cu-Kα radiation. The Pt crystallite size was calculated applying the Scherrer's equation to the (2 2 0) peak. Transmission electron microscopy (TEM) images were obtained in a JEOL 2100F microscope operated with an accelerating voltage of 200 kV and equipped with a field emission electron gun providing a point resolution of 0.19 nm. The standard procedure involved dispersing 3 mg of the sample in ethanol in an ultrasonic bath for 15 min. The sample was then placed in a Lacey carbon grid where the liquid phase was evaporated.

2.4. Electrochemical characterization

The activity of Pt/S-CXGs towards the methanol oxidation reaction (MOR) was evaluated in a half-cell system with a μAutolab Metrohm potentionstat/galvanostat. The working electrode consisted of a pyrolytic graphite disk (7 mm) with a thin layer of the electrocatalyst deposited onto it with a Pt loading of ca. 50 μg cm^{-2}. The counter electrode consisted of a pyrolytic graphite rod, while the reference electrode was a reversible hydrogen electrode (RHE). Electrochemical surface areas (ECSAs) were calculated by CO stripping. First a CO monolayer was formed by bubbling CO (99.997% Air Liquide) to the base electrolyte (a 0.5 M H_2SO_4 solution) at 0.2 V vs. RHE and subsequent removal of non-adsorbed CO by bubbling N_2 for at least 20 min. ECSAs were calculated assuming 420 μC cm^{-2} in the complete oxidation of a CO monolayer. The catalytic electrochemical activity towards the MOR was studied by cyclic voltammetry (scan rate 20 mV s^{-1}) and chronoamperometry (at 0.6 V vs. RHE during 900 s) at room temperature using deaerated 2 M CH_3OH in 0.5 M H_2SO_4 as electrolyte.

The activity of Pt/S-CXG catalysts towards the oxygen reduction reaction (ORR) was also evaluated in a half-cell system using a gas diffusion working electrode (GDWE) configuration. Gas diffusion electrodes were prepared according to a procedure described elsewhere, consisting of carbon cloth backing, gas diffusion layer and the catalytic layer under study [39]. To reduce the flooding effects, a hydrophobic backing layer was used (LT 1200W ELAT, E-TEK). The catalytic layer was composed of 33 wt.% Nafion® ionomer and 67 wt.% catalyst, with a Pt loading of 0.10 mg cm^{-2} (±0.02 mg cm^{-2}) on the basis of previous works [25,35]. The reproducibility of the data associated to the electrochemical characterization was considered by preparing and characterizing at least three electrodes for every catalyst. A mercury-mercurous sulfate (Hg/Hg_2SO_4, K_2SO_4 sat.) electrode was used as reference electrode and a high surface coiled platinum wire as counter electrode. The GDWE geometric area was 0.2 cm^2, and a 0.5 M H_2SO_4 aqueous solution was employed as electrolyte. Linear sweep voltammetries were performed at 0.5 mV s^{-1} and 25 °C flowing pure oxygen to the backing layer. Every electrochemical analysis was repeated up to stable voltammograms were obtained. The accuracy of the analyses was investigated from the standard deviation of stable curves obtained for at least three different electrodes of the same catalyst. A μAutolab Metrohm potentionstat/galvanostat was used to perform the measurements. An accelerated stress test was selected for the evaluation of the catalysts resistance to degradation, consisting of a continuous potential cycling between 0.6 and 1.2 V vs. RHE at 20 mV s^{-1} up to a total of 1000 cycles, feeding nitrogen to the electrode [40]. The evaluation of the decay process was carried out by in situ electrochemical tests: cyclic voltammetry (from 0.02 to 1.2 V vs. RHE) in nitrogen and polarization curves in pure oxygen.

3. Results and discussion

3.1. Sulfurized carbon xerogels

Table 1 shows the results of the elemental analysis for the non-treated and the sulfurized carbon xerogels (S-CXGs), as well as the notation used herein. The sulfurization procedure (see Section 2 for details) was effective introducing sulfur in the CXGs up to 7 wt.%. S-CXGs were leached with toluene, which selectively dissolves sulfur, to remove the eventual free sulfur after the thermal treatment (i.e. not incorporated to the carbon matrix). Elemental analysis of the leached toluene (not shown) resulted in only small traces of sulfur, even under the detection limit in some cases, which confirmed a high yield of the sulfurization process.

Further analysis of the sulfur species introduced in the carbon structure was gained by means of XPS of the S-CXGs. Fig. 1 shows the S 2p region of the XPS spectra for the carbon xerogel containing 4.2 wt.% S, CXG-5S, as a representative example for all the S-CXGs. The S 2p region was fitted for the S $2p_{3/2}$ and S $2p_{1/2}$ doublets, with an intensity ratio of 2:1 and spin-orbit splitting of 1.2 eV [27,41–43]. The chemical shift of this S 2p region evidences the presence of at least two chemically different sulfur species. The doublet at 164–166 eV is ascribed to the presence of either elementary sulfur or to carbon-bonded sulfur (C-S-C), whereas the doublet at 168–170 eV is related to high-valence sulfur of sulfate or sulfate-like species [26,31,32,41].

Leaching procedures in toluene revealed no traces of elementary sulfur, so we can assume that the doublet at low binding energies corresponds to carbon-bonded sulfur. Table 2 reports the quantitative analyses along with the binding energies for the S-CXGs. The contribution of the low energy peak at around 164 eV amounts to 86% of the total S 2p peak area, pointing to carbon-bonded sulfur species prevailing. This indicates also a low concentration of sulfate species that may be formed upon partial oxidation. Moreover, the ratio between the two doublets intensity (S $2p_{1/2}$ and S $2p_{3/2}$) is independent of the amount of sulfur introduced.

Such low sulfate concentration was further confirmed by means of a standardized analysis of sulfur species in coals, which resulted in sulfur concentration lower than 0.45 wt.% sulfates in the sulfurized carbon xerogels. The sulfur concentrations measured by means of XPS were significantly higher than those determined in the bulk of the samples through their elemental analysis. For example XPS of CXG-5S evidenced 8.1 at.% S (Table 2) corresponding to ca. 19 wt.% S,

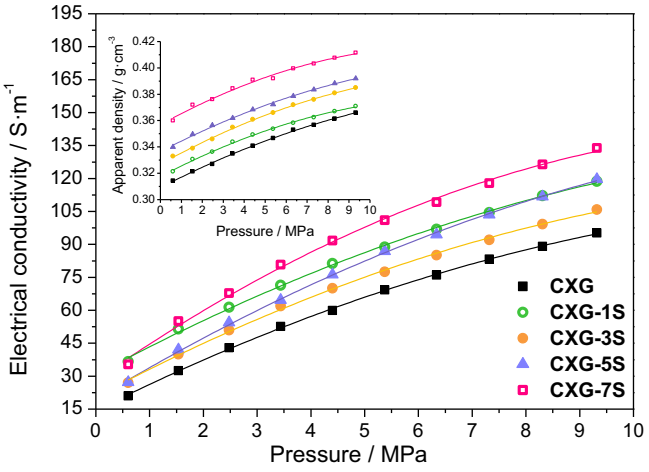

Fig. 2. Electrical conductivity and apparent density (inset) as a function of pressure of CXG and S-CXGs.

Table 3
Textural characterization parameters: surface area (S_{BET}), total pore volume (V_{pore}), micropore volume (V_{micro}), mesopore pore volume (V_{meso}) and average pore size for the S-CXGs.

Sample	S_{BET} [m^2/g]	V_{pore} [cm^3/g]	V_{micro} [cm^3/g]	V_{meso} [cm^3/g]	Av. pore size [nm]
CXG	660	1.79	0.15	1.64	23
CXG-1S	687	1.77	0.14	1.59	13
CXG-3S	570	1.56	0.09	1.38	13
CXG-5S	495	1.55	0.06	1.43	15
CXG-7S	382	1.46	0.03	1.36	18

whereas elemental analysis resulted in 4.2 wt.% (Table 1). Being XPS a surface analysis technique, this means that S is mostly present on the CXG surface. Additionally, as pointed out above, toluene leaching of the S-CXGs resulted in zero concentration of sulfur in the liquid, i.e. below detection limits, in the filtrate as well as identical sulfur content by elemental analysis of the xerogel before and after leaching procedures. All these facts point to an effective impregnation of the carbon material.

The electrical conductivity was evaluated for the bare CXG and the S-CXGs at different pressures and compaction degrees. This parameter has not been thoroughly studied in literature, although being of great importance for some kind of applications. Fig. 2 shows that the conductivity increased with S content, and as expected, it increased as well with the compaction degree, i.e. applied pressure (see Fig. 2). The apparent density progressively increased with S content, as represented in the inset of Fig. 2. This indicates that the compaction degree at a determined applied pressure increases with sulfur. The sharp increase in apparent density, explains the increase in the apparent electrical conductivity by introducing sulfur.

Textural characterization is shown in Table 3, obtained by means of the analysis of N_2 adsorption isotherms. The bare carbon xerogel possesses a well-developed porous structure, with a BET surface area of 661 $m^2\ g^{-1}$, a mean average pore size of 23 nm and a mesopore volume of 1.64 $cm^3\ g^{-1}$, corresponding to more than 90% of the total pore volume. Sulfurization results in a partial pore blockage of the porous structure, as observed from the decrease of the surface area, pore volume and the average pore size of the S-CXGs in comparison to the bare CXG one. This also explains the higher apparent density of S-CXGs resulting in higher electrical conductivity. Some studies in literature showed that S_6-S_8 molecules, formed at sulfurization temperatures below 250 °C, can only enter large pores, which may explain the decrease of the textural parameters (surface area, pore volume and average pore size) [30,31]. Upon S loading, some of the micropores of smaller pore size can also be totally blocked. The higher the amount of sulfur, the higher the probability of this happening. Given that the average pore size was calculated using the BJH method (only considering the hysteresis loop and representative of mesopores), these values are higher for those CXG with a higher S loading.

Table 4
Pt content, Pt crystallite size and electrochemically active surface area (ECSA).

Catalysts	Pt content [% wt.]	Pt crystallite size [nm]	ECSA [$m^2\ g^{-1}$ Pt]
Pt/CXG	18	3.6	39
Pt/CXG-1S	21	4.7	39
Pt/CXG-3S	20	2.8	59
Pt/CXG-5S	21	3.5	48
Pt/CXG-7S	21	< 2	25
Pt/CB-Vulcan	17	3.6	41

Table 5
Binding energies and atomic percentage of the different Pt oxidation states determined by XPS.

Catalysts	BE/eV		% at.	BE/eV		% at.	BE/eV		% at.
	$Pt4f_{7/2}$	$Pt4f_{5/2}$	Pt^0	$Pt4f_{7/2}$	$Pt4f_{5/2}$	Pt^{2+}	$P4f_{7/2}t$	$Pt4f_{5/2}$	Pt^{4+}
Pt/CXG	71.50	74.80	63.6	72.70	76.00	26.8	74.05	78.40	9.6
Pt/CXG-1S	71.40	74.80	61.0	72.11	76.00	24.8	74.04	78.00	14.2
Pt/CXG-3S	71.25	74.63	70.0	72.39	76.25	23.4	74.02	78.75	6.6
Pt/CXG-5S	71.21	74.63	63.3	72.22	76.04	26.4	74.01	78.31	10.3
Pt/CXG-7S	71.63	74.98	60.9	72.29	76.05	27.0	74.04	78.05	12.1
Pt/CB-Vulcan	71.46	74.80	61.7	72.70	76.08	26.6	74.06	78.36	12.4

3.2. Pt supported on sulfurized-carbon xerogels

Platinum nanoparticles were deposited on the CXG and S-CXG as described in the experimental section. Fig. 3 shows the TEM images acquired for the CXG- and S-CXG-supported Pt catalysts, together with the Pt particle size distribution histograms. As the sulfur content increases, Pt particles appear smaller and more evenly distributed on the surface of the CXG. Ji and co-workers claimed that sulfur acts as a metal trap, due to its strong affinity for noble metals that allows a soft acid-soft base interaction [44]. This might explain the formation of smaller particles on the S-CXG. As for the ordered mesoporous carbons synthesized by Ji et al., the S-CXG presented herein entail a better utilization of the active phase [44].

The crystallite structure of Pt/CXG catalysts was investigated by X-ray diffraction. Pt crystallite sizes, calculated applying the Scherrer's equation to the (2 2 0) reflection, are reported in Table 4. There is no clear relationship between the Pt crystallite size and the concentration of sulfur in the CXG. Indeed, the effect of sulfur on Pt crystallite size is not clear in the literature. Ahmadi and Amini reported a non-dependence of both parameters [41]. Whereas Kim and Mitani demonstrated that the presence of sulfur in the form of thiol groups (R-SH) in carbon nanotubes, reduced the crystallite size of Pt, by favoring a high dispersion of the metal precursor particles [45]. Roy also observed that the presence of sulfur favors a decrease in crystallite size [46]. Presumably, the Pt deposition method and the nature of sulfur species determine Pt crystallite size.

The surface composition of the catalysts was analyzed by XPS. The total relative amount of each Pt species along with the binding energies of every peak of the Pt-doublet are shown in Table 5. Pt^0 species are predominant, with contributions between 61 and 70%. However, there is an important contribution of oxidized Pt, as Pt^{2+} and Pt^{4+}, with about 25% contribution to Pt^{2+} and between 6 and 14% for Pt^{4+}. Also here, no clear dependence of Pt oxidation state with sulfur concentration was found. Fig. 4 shows the XPS Pt 4f profile for the different Pt/CXG catalysts. As can be noted, there is a slight shift to higher binding energies with increasing S con-

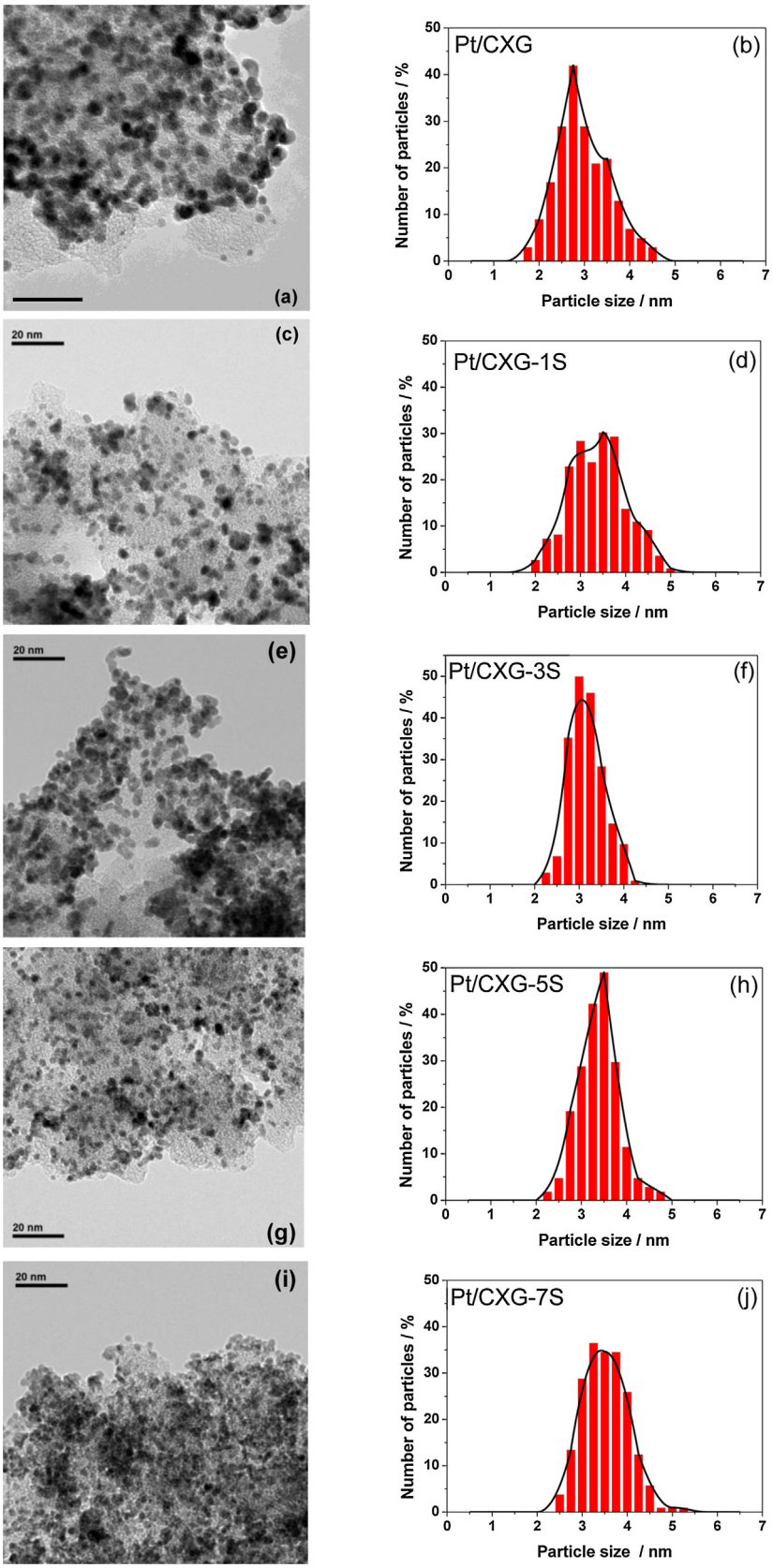

Fig. 3. TEM micrographs for the electrocatalysts: (a) Pt/CXG, (c) Pt/CXG-1S; (e) Pt/CXG-3S; (g) Pt/CXG-5S; (i) Pt/CXG-7S. Platinum particle size histograms for: (b) Pt/CXG (d) Pt/CXG-1S; (i) Pt/CXG-3S; (l) Pt/CXG-5S; (o) Pt/CXG-7S.

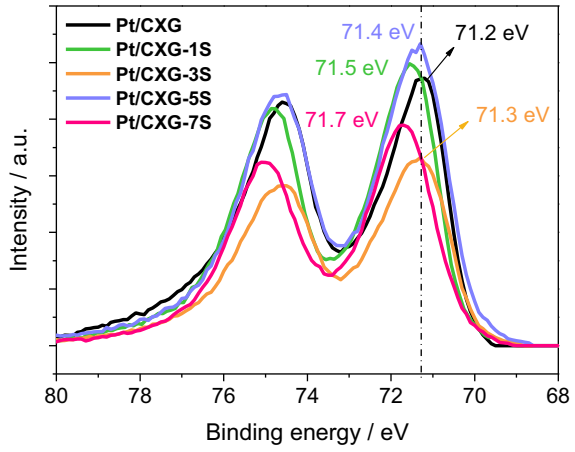

Fig. 4. XPS spectra for the Pt 4f region for Pt/S-CXG catalysts.

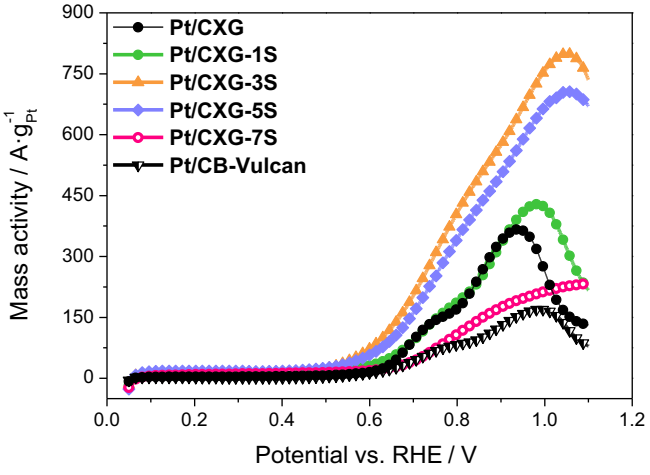

Fig. 5. Linear sweep voltammograms for the electro-oxidation of methanol (scan rate = 0.02 V s^{-1}) recorded in a 2 M CH_3OH + 0.5 M H_2SO_4 solution for Pt/S-CXG catalysts and comparison with bare CXG and Vulcan supported-catalysts.

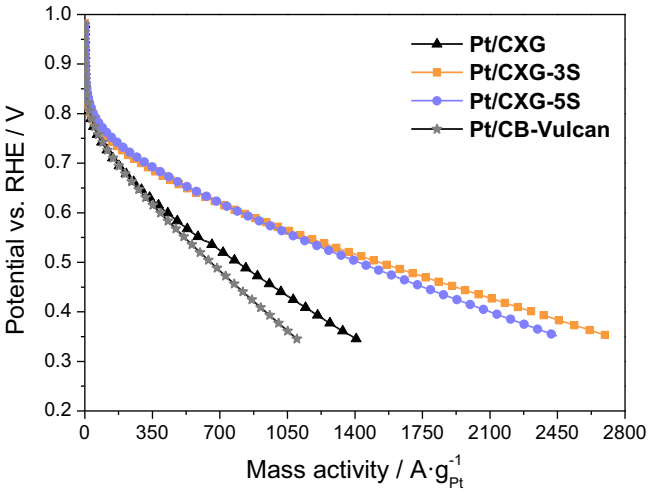

Fig. 6. ORR polarization curves obtained in half-cell with a GDWE for Pt/S-CXG catalysts and comparison with bare CXG and Vulcan supported-catalysts.

tent in the Pt 4f peak, indicating a strong interaction between Pt and S-CXG. Kim et al. found that the interaction between S and the metallic surface, changes the electronic state of the metal surface and S atoms, modifying the binding energy in the XPS [45]. This shift can be attributed to two main factors: the effect of the particle size and the ligand effect (not applicable in this case). Cheung demonstrated that the binding energy shifts to higher energies with decreasing particle size [47].

The activity of these catalysts towards the methanol electro-oxidation reaction (MOR) was investigated. The MOR is the half-reaction occurring at the anode of DMFCs. Although monometallic Pt catalysts are not the most appropriate for this reaction, the simplicity of a monometallic system was preferred, in order to properly study the role of sulfurization of the support. The results can be extrapolated to more active PtRu catalysts. Linear sweep voltammetries in 2 M CH_3OH and 0.5 M H_2SO_4 solution are shown in Fig. 5. Pt/CXGs catalysts were also compared to an in-house prepared Pt catalyst supported on commercial carbon black, Vulcan-XC-72R, which physico-chemical properties are included in Table 4. The sulfurization of CXG favors the catalytic activity towards the MOR. The maximum current density first increases with sulfur content up to the catalyst supported on CXG-3S and then decreases. Remarkably, the presence of an intermediate sulfur content (3–5 wt.%) results in a significant potential shift towards more negative values. The presence of sulfur on the carbon surface modifies the electronic state of Pt (as already corroborated by XPS), facilitating the adsorption of OH intermediates on the surface of Pt, and so increasing the rate of methanol oxidation [48]. Other studies in literature also proved that the S adsorption on Pt enhances activity in formic acid, formaldehyde, and methanol (MeOH) electrooxidation reactions [49,50]. According to this studies, the S adsorption on Pt catalyst, increases the attraction of the CH_3 group of the CH_3OH molecule, enhancing its decomposition by enhancing the parallel reaction pathway of methanol decomposition. We also encountered that the electrochemically active surface area (ECSA) of the catalyst, reported in Table 4, influenced the methanol oxidation rate. As a result, the catalyst Pt/CXG-3S presents the highest catalytic activity, due to the balance between a good intrinsic activity and a high ECSA. In any case, catalysts supported on S-CXGs are more active towards MOR than the catalyst supported on the bare CXG and than the catalyst supported on Vulcan, (only Pt/CXG-7S shows a poorer activity, due to its lower ECSA, 25 m^2 g^{-1}). It appears that there is an optimum sulfur content of about 3 wt.% that maximizes MOR activity. As in the present study, Park et al. also found optimal amounts of S coverage enhancing methanol oxidation [51]. To sum up, the higher catalytic activity of catalysts supported on S-CXGs might be ascribed to two effects: a better metallic dispersion and a better intrinsic activity.

In recent years, increasing works deal with doping or functionalization of carbonaceous materials with sulfur as a way to improve the catalytic performance of supported catalysts for the ORR [27,45,46,52,53]. Considering the previous results obtained for the MOR, the Pt-catalysts supported on CXG with 3 wt.% and 5 wt.% of sulfur, along with the catalyst supported on the bare xerogel, were selected for the study of the ORR. These catalysts presented crystallite sizes between 2.8 and 3.6 nm. Pt crystallite size has a relevant importance on the ORR mass activity [52]. Kinoshita et al. established that the optimum crystallite size of Pt-catalysts for the ORR to obtain the maximal activity was around 3 nm [52]. Pt/CXG catalysts were compared to the in-house prepared Pt catalyst supported on commercial carbon black, Vulcan-XC-72R. Fig. 6 shows the ORR polarization curves obtained in a gas diffusion-working electrode (GDWE) configuration in a 0.5 M H_2SO_4 solution, flowing pure O_2 to the backing layer of the electrode. The sulfurization of the carbon xerogel significantly improves the performance of the catalyst, being Pt/CXG-3S slightly more active than Pt/CXG-5S. Although crystallite sizes for catalysts Pt/CXG and Pt/CXG-5S are very similar, metal dispersion and ECSA improve with the pres-

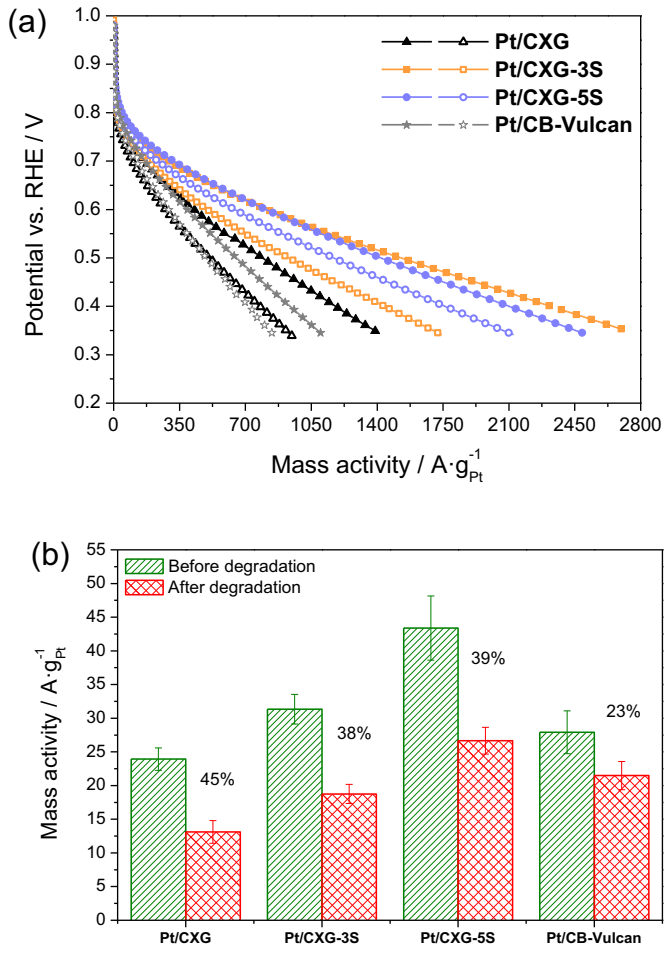

Fig. 7. (a) ORR polarization curves before (filled symbols) and after (empty symbols) degradation tests. (b) ORR mass activity at 0.8 V vs. RHE before and after degradation tests. The percentages indicate the relative loss of activity.

ence of sulfur, resulting in a higher catalytic activity, which follows the order of the ECSA (see Table 4).

Accelerated degradation tests were also carried out in order to investigate the durability of Pt/CXG catalysts. Potential cycling was performed to evaluate the resistance to platinum sintering and dissolution [54]. 1000 cycles between 0.6 V and 1.2 V (vs. RHE) at a scan rate of 20 mV s^{-1} were performed, feeding an inert gas to the GDWE in 0.5 M H_2SO_4 as electrolyte.

Fig. 7a shows the ORR polarization curves before and after the degradation tests. The Pt catalysts supported on S-CXGs are more active than those supported on the reference materials before and after the degradation tests. The catalyst supported on the commercial carbon support, Pt/Vulcan presented the lowest loss of ORR electrochemical activity. It is well-known that surface area, structural ordering degree and surface chemistry of the carbon support influence its corrosion rate [55–57]. Vulcan is characterized by a low BET surface area (250 m^2 g^{-1}) compared to CXGs (≈380–690 m^2 g^{-1}). The low relative loss of activity of Pt/Vulcan can thus be attributed to its low surface area. Fig. 7b shows the ORR mass activity in the activation controlled region (at 0.8 V vs. RHE) before and after the degradation tests. The standard deviation associated to data reproducibility is indicated by error bars in the figure, accounting for less than 15% of error. Even if the relative loss of performance after degradation of Pt/CXG catalysts is yet higher than of Pt/Vulcan, the sulfurization reduces the percentual decay from 45% (Pt/CXG) to 38–39% (Pt/CXG-3S–Pt/CXG-5S). This could be related to either the lower BET surface area of the support (Table 3) and/or a better metal-support interaction in the presence of sulfur moieties. In any case, this indicates that the simple sulfurization method of the support presented herein represents a good strategy to slightly improve the resistance of Pt-based catalysts to corrosion.

4. Conclusions

The simple sulfurization of carbon xerogels with elemental sulfur leads to the effective introduction of sulfur moieties bonded to the carbon surface. The introduction of sulfur in the carbonaceous matrix increases its electrical conductivity, due to an increased density of the material, but it occurs a partial pore blockage that slightly modifies the BET surface area

Pt nanoparticles have been supported on S-CXGs by an impregnation method. The presence of sulfur on the support leads to lower crystallite sizes of Pt particles and improved metallic dispersion.

Pt catalysts supported on S-CXGs showed enhanced catalytic activity towards both the methanol oxidation reaction and the oxygen reduction reaction, due to their higher ECSA, consequence of the lower crystal size and better metallic dispersion of Pt nanoparticles. Catalysts supported on S-CXGs exceeded not only the performance of the catalyst supported on the bare xerogel, but also the catalyst supported on the commercial support, Vulcan. Pt-catalysts supported on sulfur-doped CXGs also presented a slightly increased resistance towards the corrosion processes. The simple method of sulfurization on carbon xerogels has proved to be an effective method to increase both activity and durability.

Acknowledgements

The authors wish to thank the Spanish Ministry of Economy and Competitiveness (Secretaría de Estado de I+D+I) and FEDER for financial support under the project CTQ2011-28913-C02-01.

References

[1] A.S. Aricò, V. Baglio, V. Antonucci, Direct Methanol Fuel Cells, Nova Science Publishers Inc., New York USA, 2010.
[2] A.S. Aricò, V. Baglio, V. Antonucci, J. Zhang, H. Liu, Electrocatalysis of direct methanol fuel cells, Fundam. Appl. (2009).
[3] A.S. Aricò, V.V. Baglio Antonucci, Nanotechnology for the Energy Challenge, Wiley-VCH Verlag GmbH & Co KGaA, Weinheim, Germany, 2010.
[4] A. Hamnett, in: Wolf Vielstich, Arnold Lamm, Hubert A. Gasteiger (Eds.), Handbook of Fuel Cells: Fundamentals, Technology, Applications, 4-Volume Set, John Wiley & Sons Chichester, West Sussex, PO19 8SQ United Kingdom, 2009.
[5] S. Sharma, B.G. Pollet, Support materials for PEMFC and DMFC electrocatalysts—a review, J. Power Sources 208 (2012) 96–119.
[6] S. Siracusano, A. Stassi, E. Modica, V. Baglio, A.S. Aricò, Preparation and characterisation of Ti oxide based catalyst supports for low temperature fuel cells, Int. J. Hydrogen Energy 38 (2013) 11600–11608, http://dx.doi.org/10.1016/j.ijhydene.2013.04.161.
[7] M. Roca-Ayats, G. García, J.L. Galante, M.A. Peña, M.V. Martínez-Huerta, Electrocatalytic stability of Ti based-supported Pt3Ir nanoparticles for unitized regenerative fuel cells, Int. J. Hydrogen Energy 39 (2014) 5477–5484, http://dx.doi.org/10.1016/j.ijhydene.2013.12.187.
[8] Z. Yang, H. Nie, X. Chen, X. Chen, S. Huang, Recent progress in doped carbon nanomaterials as effective cathode catalysts for fuel cell oxygen reduction reaction, J. Power Sources 236 (2013) 238–249, http://dx.doi.org/10.1016/j.jpowsour.2013.02.057.
[9] S. Shahgaldi, J. Hamelin, Improved carbon nanostructures as a novel catalyst support in the cathode side of PEMFC: a critical review, Carbon N. Y. 94 (2015) 705–728.
[10] E. Antolini, Carbon supports for low-temperature fuel cell catalysts, Appl. Catal. B Environ. 88 (2009) 1–24, http://dx.doi.org/10.1016/j.apcatb.2008.09.030.
[11] D. Higgins, M.A. Hoque, M.H. Seo, R. Wang, F. Hassan, J.-Y. Choi, et al., Development and simulation of sulfur-doped graphene supported platinum with exemplary stability and activity towards oxygen reduction, Adv. Funct. Mater. 24 (2014) 4325–4336, http://dx.doi.org/10.1002/adfm.201400161.
[12] J.L. Figueiredo, M.F.R. Pereira, P. Serp, P. Kalck, P.V. Samant, J.B. Fernandes, Development of carbon nanotube and carbon xerogel supported catalysts for

the electro-oxidation of methanol in fuel cells, Carbon N. Y. 44 (2006) 2516–2522, http://dx.doi.org/10.1016/j.carbon.2006.05.033.
[13] E. Antolini, Formation, microstructural characteristics and stability of carbon supported platinum catalysts for low temperature fuel cells, J. Mater. Sci. 38 (2016) 2995–3005 (n.d.).
[14] E. Antolini, Carbon supports for low-temperature fuel cell catalysts, Appl. Catal. B Environ. 88 (2009) 1–24, http://dx.doi.org/10.1016/j.apcatb.2008.09.030.
[15] C. Lin, J.A. Ritter, Effect of synthesis pH on the structure of carbon xerogels, Carbon N. Y. 35 (1997) 1271–1278.
[16] J.L. Figueiredo, M.F.R. Pereira, Synthesis and functionalization of carbon xerogels to be used as supports for fuel cell catalysts, J. Energy Chem. 22 (2013) 195–201.
[17] S.A. Al-Muhtaseb, J.A. Ritter, Preparation and properties of resorcinol-formaldehyde organic and carbon gels, Adv. Mater. 15 (2003) 101–114.
[18] N. Job, S. Lambert, A. Zubiaur, C. Cao, J.-P. Pirard, Design of Pt/Carbon xerogel catalysts for PEM fuel, Cells Catal. 5 (2015) 40–57.
[19] C. Alegre, L. Calvillo, R. Moliner, J.A. González-Expósito, O. Guillén-Villafuerte, M.V.M. Huerta, et al., Pt and PtRu electrocatalysts supported on carbon xerogels for direct methanol fuel cells, J. Power Sources 196 (2011) 4226–4235.
[20] P.V. Samant, C.M. Rangel, M.H. Romero, J.B. Fernandes, J.L. Figueiredo, Carbon supports for methanol oxidation catalyst, J. Power Sources 151 (2005) 79–84.
[21] C. Arbizzani, S. Beninati, E. Manferrari, F. Soavi, M. Mastragostino, Cryo- and xerogel carbon supported PtRu for DMFC anodes, J. Power Sources 172 (2007) 578–586.
[22] M. Ouattara-Brigaudet, S. Berthon-Fabry, C. Beauger, M. Chatenet, N. Job, M. Sennour, et al., Influence of the carbon texture of platinum/carbon aerogel electrocatalysts on their behavior in a proton exchange membrane fuel cell cathode, Int. J. Hydrogen Energy 37 (2012) 9742–9757.
[23] F. Maillard, N. Job, M. Chatenet, in: S. Suib (Ed.), New and Future Developments in Catalysis. Batteries, Hydrogen Storage and Fuel Cells, Elsevier, 2013, 2016, ISBN :9780444538802.
[24] C. Alegre, E. Baquedano, M.E. Gálvez, R. Moliner, M.J. Lázaro, Tailoring carbon xerogels' properties to enhance catalytic activity of Pt catalysts towards methanol oxidation, in: I, nt. J. Hydrogen Energy (2015).
[25] C. Alegre, D. Sebastián, E. Baquedano, M.E. Gálvez, R. Moliner, M. Lázaro, Tailoring synthesis conditions of carbon xerogels towards their utilization as Pt-catalyst supports for oxygen reduction reaction (ORR), Catalysts 2 (2012) 466–489.
[26] W. Kiciński, M. Szala, M. Bystrzejewski, Sulfur-doped porous carbons: synthesis and applications, Carbon N. Y. 68 (2014) 1–32.
[27] W.S. Baker, J.W. Long, R.M. Stroud, D.R. Rolison, Sulfur-functionalized carbon aerogels: a new approach for loading high-surface-area electrode nanoarchitectures with precious metal catalysts, J. Non. Cryst. Solids 350 (2004) 80–87.
[28] S.-A. Wohlgemuth, R.J. White, M.-G. Willinger, M.-M. Titirici, M. Antonietti, A one-pot hydrothermal synthesis of sulfur and nitrogen doped carbon aerogels with enhanced electrocatalytic activity in the oxygen reduction reaction, Green Chem. 14 (2012) 1515.
[29] W. Kiciński, A. Dziura, Heteroatom-doped carbon gels from phenols and heterocyclic aldehydes: sulfur-doped carbon xerogels, Carbon N. Y. 75 (2014) 56–67.
[30] W. Liu, R.D. Vidić, T.D. Brown, Optimization of sulfur impregnation protocol for fixed-bed application of activated carbon-based sorbents for gas-phase mercury removal, Environ. Sci. Technol. 32 (1998) 531–538 http://pubs.acs.org/doi/abs/10.1021/es970630%2B.
[31] H.-C. Hsi, M.J. Rood, M. Rostam-Abadi, S. Chen, R. Chang, Effects of sulfur impregnation temperature on the properties and mercury adsorption capacities of activated carbon fibers (ACFs), Environ. Sci. Technol. 35 (2001) 2785–2791.
[32] M. Rao, W. Li, E.J. Cairns, Porous carbon-sulfur composite cathode for lithium/sulfur cells, Electrochem. Commun. 17 (2012) 1–5.
[33] O. Czakkel, K. Marthi, E. Geissler, K. László, Influence of drying on the morphology of resorcinol–formaldehyde-based carbon gels, Micropor. Mesopor. Mater. 86 (2005) 124–133.
[34] H.F. Gorgulho, F. Gonçalves, M.F.R. Pereira, J.L. Figueiredo, Synthesis and characterization of nitrogen-doped carbon xerogels, Carbon N. Y. 47 (2009) 2032–2039.
[35] D. Sebastián, C. Alegre, M.E. Gálvez, R. Moliner, M.J. Lázaro, A.S. Aric&#x00F2, et al., Towards new generation fuel cell electrocatalysts based on xerogel–nanofiber carbon composites, J. Mater. Chem. A 2 (2014) 13713 (accessed 17.03.16) http://pubs.rsc.org/en/content/articlehtml/2014/ta/c4ta02108h.
[36] E. Antolini, Structural parameters of supported fuel cell catalysts: the effect of particle size, inter-particle distance and metal loading on catalytic activity and fuel cell performance, Appl. Catal. B Environ. 181 (2016) 298–313 (accessed 24.8.15) http://www.sciencedirect.com/science/article/pii/S0926337315300801.
[37] D. Sebastián, A.G. Ruiz, I. Suelves, R. Moliner, M.J. Lázaro, On the importance of the structure in the electrical conductivity of fishbone carbon nanofibers, J. Mater. Sci. 48 (2012) 1423–1435.
[38] A. Celzard, J.F. Marêché, F. Payot, G. Furdin, Electrical conductivity of carbonaceous powders, Carbon N. Y. 40 (2002) 2801–2815.
[39] V. Baglio, A. Di Blasi, A.S. Aricò, V. Antonucci, P.L. Antonucci, F. Nannetti, et al., Investigation of the electrochemical behaviour in DMFCs of chabazite and clinoptilolite-based composite membranes, Electrochim. Acta 50 (2005) 5181–5188.
[40] R. Borup, J. Meyers, B. Pivovar, Y.S. Kim, R. Mukundan, N. Garland, et al., Scientific aspects of polymer electrolyte fuel cell durability and degradation, Chem. Rev. 107 (2007) 3904–3951.
[41] R. Ahmadi, M.K. Amini, Synthesis and characterization of Pt nanoparticles on sulfur-modified carbon nanotubes for methanol oxidation, Int. J. Hydrogen Energy 36 (2011) 7275–7283.
[42] K.E. Swider, The chemical state of sulfur in carbon-supported fuel-cell electrodes, J. Electrochem. Soc. 143 (1996) 813.
[43] M.E. Labib, J.H. Thomas, D.D. Embert, The effect of heat treatment on sulfur in an electrically-conductive carbon black, Carbon N. Y. 22 (1984) 445–451.
[44] X. Ji, K.T. Lee, R. Holden, L. Zhang, J. Zhang, G.A. Botton, et al., Nanocrystalline intermetallics on mesoporous carbon for direct formic acid fuel cell anodes, Nat. Chem. 2 (2010) 286–293.
[45] Y. Kim, T. Mitani, Surface thiolation of carbon nanotubes as supports: a promising route for the high dispersion of Pt nanoparticles for electrocatalysts, J. Catal. 238 (2006) 394–401.
[46] S.C. Roy, Direct methanol fuel cell cathodes with sulfur and nitrogen-based carbon functionality, J. Electrochem. Soc. 143 (1996) 3073.
[47] T.T.P. Cheung, X-ray photoemission of small platinum and palladium clusters, Surf. Sci. 140 (1984) 151–164, http://dx.doi.org/10.1016/0039-6028(84)90388-1.
[48] D. Sebastian, A. Stassi, S. Siracusano, C.L. Vecchio, A.S. Arico, V. Baglio, Influence of metal oxide additives on the activity and stability of PtRu/C for methanol electro-oxidation, J. Electrochem. Soc. 162 (2015) F713–F717.
[49] S. Chen, T. Noles, M. Schell, Differences in oscillations and sequences of dynamical states caused by anion adsorption in the electrochemical oxidation of formic acid, J. Phys. Chem. A 104 (2000) 6791–6798, http://dx.doi.org/10.1021/jp001066j.
[50] I.-S. Park, D.O. Atienza, A.M. Hofstead-Duffy, D. Chen, Y.J. Tong, Mechanistic insights on sulfide-adsorption enhanced activity of methanol electro-oxidation on Pt nanoparticles, ACS Catal. 2 (2012) 168–174, http://dx.doi.org/10.1021/cs200546f.
[51] I.-S. Park, D.O. Atienza, A.M. Hofstead-Duffy, D. Chen, Y.J. Tong, Mechanistic insights on sulfide-adsorption enhanced activity of methanol electro-oxidation on Pt nanoparticles, ACS Catal. 2 (2012) 168–174 (accessed 22.3.16) http://dx.doi.org/10.1021/cs200546f.
[52] K. Kinoshita, Particle size effects for oxygen reduction on highly dispersed platinum in acid electrolytes, J. Electrochem. Soc. 137 (1990) 845.
[53] D.-T. Chin, Hydrogen sulfide poisoning of platinum anode in phosphoric acid fuel cell electrolyte, J. Electrochem. Soc. 133 (1986) 2447.
[54] A. Stassi, E. Modica, V. Antonucci, A.S. Aricò, A half cell study of performance and degradation of oxygen reduction catalysts for application in low temperature fuel cells, Fuel Cells 9 (2009) 201–208.
[55] P.L. Antonucci, F. Romeo, M. Minutoli, E. Alderucci, N. Giordano, Electrochemical corrosion behavior of carbon black in phosphoric acid, Carbon N. Y. 26 (1988) 197–203.
[56] N. Giordano, P.L. Antonucci, E. Passalacqua, L. Pino, A.S. Aricò, K. Kinoshita, Relationship between physicochemical properties and electrooxidation behaviour of carbon materials, Electrochim. Acta 36 (1991) 1931–1935.
[57] K. Artyushkova, S. Pylypenko, M. Dowlapalli, P. Atanassov, Structure-to-property relationships in fuel cell catalyst supports: correlation of surface chemistry and morphology with oxidation resistance of carbon blacks, J. Power Sources. 214 (2012) 303–313.